Two crystal structures of pectin lyase A from *Aspergillus* reveal a pH driven conformational change and striking divergence in the substrate-binding clefts of pectin and pectate lyases

O Mayans[1], M Scott[1], I Connerton[1], T Gravesen[2], J Benen[3], J Visser[3], R Pickersgill[1]* and J Jenkins[1]*

Background: Microbial pectin and pectate lyases are virulence factors that degrade the pectic components of the plant cell wall. The homogalacturan backbone of pectin varies in its degree of methylation from the highly methylated and relatively hydrophobic form known as pectin, to the fully demethylated and highly charged form known as pectate. Methylated and demethylated regions of pectin are cleaved by pectin lyase and calcium-dependent pectate lyases, respectively. Protein engineering of lyases specific for particular patterns of methylation, will yield modified pectins of high value to the food and pharmaceutical industries.

Results: The crystal structures of pectin lyase A from two strains of *Aspergillus niger,* N400 and 4M-147, have been determined at pH 6.5 (2.4 Å resolution) and pH 8.5 (1.93 Å resolution), respectively. The structures were determined by a combination of molecular replacement, multiple isomorphous replacement and intercrystal averaging. Pectin lyase A folds into a parallel β helix and shares many of the structural features of pectate lyases, despite no more than 17% sequence identity after pairwise structure-based alignment. These shared structural features include amino acid stacks and the asparagine ladder. However, the differences in the substrate-binding clefts of these two enzymes are striking. In pectin lyase A, the cleft is dominated by aromatic residues and is enveloped by negative electrostatic potential. In pectate lyases, this cleft is rich in charged residues and contains an elongated ribbon of positive potential when Ca^{2+} is bound. The major difference between the two pectin lyase A structures from the two strains is in the conformation of the loop formed by residues 182–187. These observed differences are due to the different pH values of crystallization.

Conclusions: The substrate-binding clefts and catalytic machinery of pectin and pectate lyases have diverged significantly. Specificity is dictated by both the nature of the protein–carbohydrate interaction and long-range electrostatic forces. Three potential catalytic residues have been identified in pectin lyase, two of these are common to pectate lyases. Pectin lyase A does not bind Ca^{2+} but an arginine residue is found in an equivalent position to the Ca^{2+} ion in pectate lyase, suggesting a similar role in catalysis. The activity of pectin lyase A is pH-dependent with an optimum activity at pH 5.5. The activity drops above pH 7.0 due to a conformational change at the binding cleft, triggered by the proximity of two buried aspartate residues.

Addresses: [1]Department of Food Macromolecular Science, Institute of Food Research, Earley Gate, Whiteknights Road, Reading RG6 6BZ, UK, [2]Danisco Ingredients, Edwin Rahrs Vej 38, DK-8220 Brabrand, Denmark and [3]Section of Molecular Genetics of Industrial Microorganisms, Wageningen Agricultural University, Dreijenlaan-2, NL-6703 HA Wageningen, The Netherlands.

*Corresponding authors.
E-mail: john.jenkins@bbsrc.ac.uk
richard.pickersgill@bbsrc.ac.uk

Key words: crystal structure, parallel β helix, pectin lyase, pH conformational change, substrate specificity

Received: 4 February 1997
Revisions requested: 27 February 1997
Revisions received: 19 March 1997
Accepted: 7 April 1997

Structure 15 May 1997, 5:677–689
http://biomednet.com/elecref/0969212600500677

Introduction

Pectate (E.C. 4.2.2.9) and pectin lyases (E.C. 4.2.2.10) are produced by bacteria and fungi [1] and genes encoding related proteins are found in many plants [2,3]. These enzymes cleave α-1,4 links between galacturonosyl residues in the pectic component of the primary cell wall and middle lamella of higher plants. Enzymatic cleavage occurs via a β-elimination reaction resulting in the formation of an unsaturated C4–C5 bond at the nonreducing end of the cleaved polysaccharide. Pectate lyases are more specific for demethylated or low-esterified forms of pectin, require Ca^{2+} for activity and most have a pH optimum near 8.5. In contrast, pectin lyases are specific for highly methylated forms of the substrate, do not require Ca^{2+} for activity and the pH optimum is generally close to 5.5.

Extracellular secretion of pectinolytic enzymes by microorganisms is known to play a major role in phytopathogenesis. Plant pathogens produce an array of enzymes capable of attacking the plant cell wall components. However, a convincing role in plant disease has only been established for those enzymes that attack the pectic fraction [4,5]. The depolymerization of the pectic components of the cell wall leads to tissue maceration and cell death, as occurs in the soft-rotting of living plant tissue and the decay of harvested crops. Understanding the molecular basis for substrate specificity and the mode of action of pectinases will aid the design of inhibitors for preventing plant disease.

Microbial pectinolytic enzymes are also produced on a large scale as processing aids for the food industry [1,6]. Pectinases are becoming essential tools for the analysis and modification of pectins. The rational design of pectinases would enable the development of dedicated enzyme cocktails and optimized substrates which would innovate pectin manufacturing.

The extracellular family of pectate lyases shares sequence similarities with pectin lyases [7], suggesting that they may have evolved from a common ancestral lyase. Given the sequence relation a similar topology is expected for both pectate and pectin lyases, and as they catalyze similar β-elimination reactions on closely related substrates a related mechanism might be expected.

To date, the crystal structures of three pectate lyases have been determined: pectate lyase C (PelC) [8] and pectate lyase E (PelE) [9] (both from *Erwinia chrysanthemi*) and the pectate lyase from *Bacillus subtilis* (BsPel) complexed with Ca^{2+} [10]. The structures comprise a right-handed parallel β-helix domain and a major loop region. These structures have allowed the identification of the pectinolytic substrate-binding site and several putative catalytic residues. Ca^{2+} is essential for the activity of all pectate lyases but its role in substrate binding and catalysis is not yet understood. Prior to the structural studies, it was believed that Ca^{2+} simply cross-linked the strands of the substrate into a structure that can be recognized by the enzyme [11]. However, the Ca^{2+}–BsPel complex provides direct evidence that Ca^{2+} binds to the enzyme. In this structure, Ca^{2+} binds at the bottom of a pronounced cleft to three aspartate residues, generating a ribbon of positive electrostatic potential complementary to the negatively charged, polymeric pectate substrate. Given that pectate lyases are inactive in the absence of Ca^{2+}, the Ca^{2+}-binding site has been proposed as the active site and the cleft in which it is located has been proposed as the substrate-binding site. A recent structure-based study of sequence conservation [7] around the Ca^{2+}-binding site, revealed that Asp184 and Arg279 (BsPel numbering) are invariant amino acids across the pectate and pectin lyase family. These two residues are, therefore, expected to play a critical role in catalysis.

Site-directed mutagenesis studies [12] have confirmed that the pectinolytic active site includes the region around the Ca^{2+}-binding site. However, a second cluster of conserved amino acids has been identified [7] at the opposite side of the parallel β helix, in a region of high structural conservation containing the *Val*-Trp-*Ile*-Asp-His pattern (conservatively substituted residues are shown italicised, non-italicised residues are absolutely conserved). It has been proposed [7,12] that this conserved region constitutes a second active site of yet unidentified function.

It is expected that the mechanism of pectin lyases will be related to that of pectate lyases although the former does not require Ca^{2+} for activity. To gain an understanding of the carbohydrate recognition strategy and catalysis by β-elimination in pectinolytic enzymes, we have determined the X-ray crystal structures of pectin lyase A from two strains of *Aspergillus niger* (N400 and 4M-147) to a resolution of 2.4 Å and 1.93 Å, respectively. The protein sequences from these two strains differ in nine amino acid substitutions: Glu12→Lys, Asp19→Ser, Val101→Thr, Gly213→Ala, Cys248→Ala, Phe253→Trp, Ala289→Glu, Thr296→Ser and Cys317→Ser (from strain N400 to strain 4M-147, numbered from the N terminus of the mature protein). The structures were solved by molecular replacement (MR), multiple isomorphous replacement (MIR) and intercrystal averaging techniques. Pectin lyase A from strain N400 was crystallized at the active pH of 6.5, while the enzyme from strain 4M-147 corresponds to a less active form at pH 8.5 [13]. The structural differences observed between the two models will provide an insight into the effect of pH on activity.

Results and discussion

Overall architecture

The structures of pectin lyase A from strains N400 and 4M-147 include all 359 residues of the mature protein and solvent molecules, as listed in Table 1. The common overall architecture consists of a parallel β-helix domain and a loop region (Fig. 1). The overall folds of the two structures are also shown as Cα traces in Figure 2. As seen in the pectate lyases, PelC, PelE and BsPel [14], parallel β strands fold into a large, right-handed helix, which is dimpled in cross-section. The β strands of consecutive turns line up to form three parallel β sheets called PB1, PB2 and PB3. PB1 and PB2 form an antiparallel β sandwich, while PB3 lies approximately perpendicular to PB2. PB1 is formed by eight β strands and PB2 and PB3 by nine β strands each. The β strands are generally short, typically three amino acids for PB1, four or five amino acids for PB2 and three to five for PB3. The β sheets generate eight complete turns in the parallel β helix plus one additional, incomplete N-terminal turn formed by the first β strand of PB2 and PB3.

Table 1

Refinement statistics.

Source	*A. niger* 4M-147	*A. niger* N400
Space group	$P2_12_12_1$	P1
Resolution range (Å)	15–1.9	33.3–2.4
No. of reflections	23 147§	23 252
R factor (%)*	19.6	18.9
R_{free} (%)	23.0	22.6
Asymmetric unit		
no. of molecules	1	2
no. of protein atoms (non-hydrogen)	2675	2671×2
no. of solvent atoms	183	138
Rmsd bond length (Å)†	0.008	0.007
Rmsd bond angles (°)†	1.77	1.45
Overall G factor‡	+0.16	+0.19
Ramachandran plot‡		
most favoured regions (%)	80.1	80.0
additionally allowed (%)	18.0	18.4
generously allowed (%)	1.6	1.3
disallowed regions	0	1¶
Average B factors (Å²)		
mainchain	33.7	36.1
all atoms (no water)	34.5	37.1

*R factor = $\Sigma|F_{obs}-F_{calc}|/\Sigma F_{obs}$. †Root mean square deviation. ‡Geometrical factor and Ramachandran details as defined in PROCHECK [33]. §For this strain only, reflections where ($F > 2\sigma(F)$) were used. ¶Asp242 was the residue in the disallowed region of the Ramachandran plot.

Figure 1

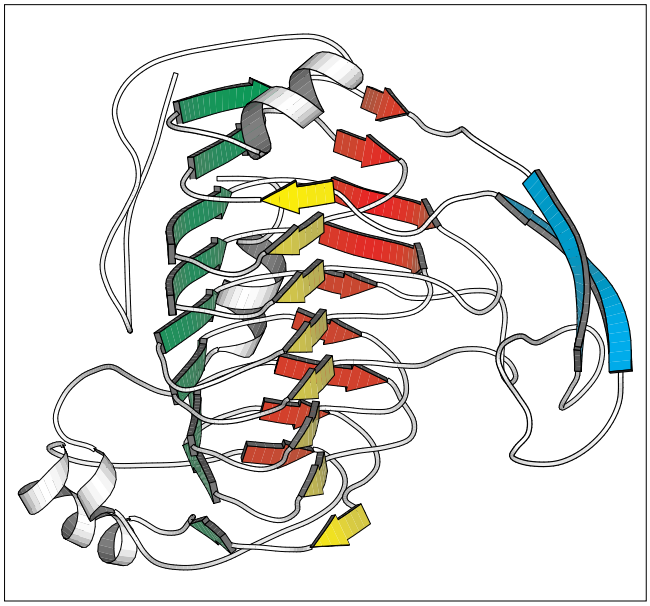

The overall architecture of pectin lyase A from strain 4M-147. A schematic representation in which arrows represent β strands and coils represent α helices. Parallel β sheet 1 (PB1) is shown in yellow, PB2 is in green and PB3 is in red. The antiparallel β sheet in the long T3 loop is shown in blue. (Figure prepared using MOLSCRIPT [34].)

Both ends of the parallel β domain are capped: the N-terminal end of the cylinder is capped by a short α helix, which is conserved in the structures of the three pectate lyases determined to date; the C-terminal end is capped by a polypeptide chain in extended conformation.

The turns between β sheets have been referred to as T1 (between PB1 and PB2), T2 (between PB2 and PB3) and T3 (between PB3 and PB1). T1 is of the β arch type. The T2 turn introduces a change of 90° in the direction of the polypeptide backbone. The turn is commonly composed of two residues, C_i and C_{i+1}, of which C_i is in α_L conformation, typically a glycine or asparagine, and C_{i+1} is an asparagine in five of these turns, forming the asparagine ladder described below. The T3 loops are commonly lengthy and of more complex conformation, constituting the major loop region. They protrude from the central parallel β helix, packing against PB1 and forming the substrate-binding cleft. In pectin lyase A, the T3 loop region is dominated by a single loop that protrudes prior to the first turn of the parallel β helix. This T3 loop begins and ends with two β strands, residues 57–63 and 91–97, which form an antiparallel β sheet. The middle part of the loop is markedly convoluted, its structure being supported by two disulphide bridges, Cys63–Cys82 and Cys72–Cys206. Three of the cysteine residues involved are part of this same loop (Cys63, Cys72 and Cys82) while a fourth (Cys206) is situated in the fourth T3 loop. The latter loop, of medium length, forms part of the bottom of the substrate-binding cleft.

Although the major loop region in pectin lyase is formed by T3 loops, there is a second, minor loop area at the C-terminal end of the parallel β helix. This is formed by two loops and includes two short helices with rather distorted hydrogen-bond patterns, which pack against each other. The major helix is part of the long T2 loop from the eighth turn of the parallel β helix domain; this T2 loop conformation is maintained by a disulphide bridge (Cys302–Cys310). The minor helix is part of the C-terminal tail.

A typical characteristic of the interior of the parallel β-helix domain, is that the sidechains of residues at corresponding positions in consecutive β strands stack directly upon each other. As previously reported for pectate lyases, a distinct asparagine ladder appears in the inner position of the T2 turn in the core of the helix. In the pectin lyase A structure, this ladder is composed of five residues, while four asparagines are present in the ladder of BsPel, six in PelC and only three in PelE. An inner aromatic stack is also present, composed of three residues (two phenylalanines and one tryptophan in strain 4M-147, and three phenylalanines in N-400), and located on the C-terminal three turns of the parallel β helix. Four aliphatic stacks are also noticeable in the core. Some sidechains that are oriented outwards into the solvent are stacked as well: a striking example is the clustering of five tyrosine residues at the back of the substrate-binding site, where the conserved C-terminal tail packs against the T2 turn. This exterior stack is partially

Figure 2

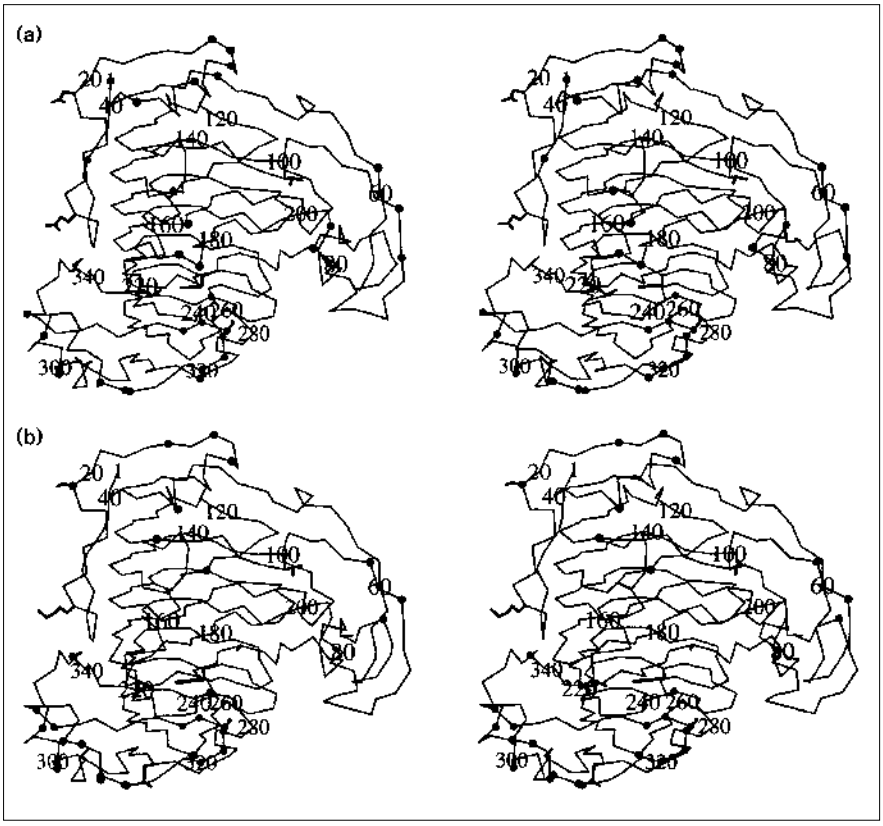

Stereo view Cα trace of pectin lyase A from strains N400 (a) and 4M-147 (b). The nine amino acid substitutions (Glu12→Lys, Asp19→Ser, Val101→Thr, Gly213→Ala, Cys248→Ala, Phe253→Trp, Ala289→Glu, Thr296→Ser and Cys317→Ser, from strain N400 to strain 4M-147) are drawn as stick models. A solid circle indicates that a residue is involved in a crystal contact (calculated using CONTACT [22] and a contact distance of 4.0 Å). (Figure prepared using MOLSCRIPT [34].)

conserved, although less prominent, in BsPel and PelC. Stacks of residues are illustrated in Figures 3a and 3b.

The conformation of the N- and C-terminal tails is closely related to that observed in the pectate lyase structures. The N-terminal tail packs against PB2 while the C-terminal tail, comprising a highly conserved, amphipathic α helix, lies across PB3 and packs against the T2 turn . In general, PB2 and PB3 constitute the area of highest structural conservation, which is at a maximum in the asparagine ladder in T2 and the *Val*-Trp-*Ile*-Asp-His pattern in PB2. It should be noted that the high structural conservation occurs in regions distant from the active site, while the binding cleft and surroundings constitute the most divergent part of the

Figure 3

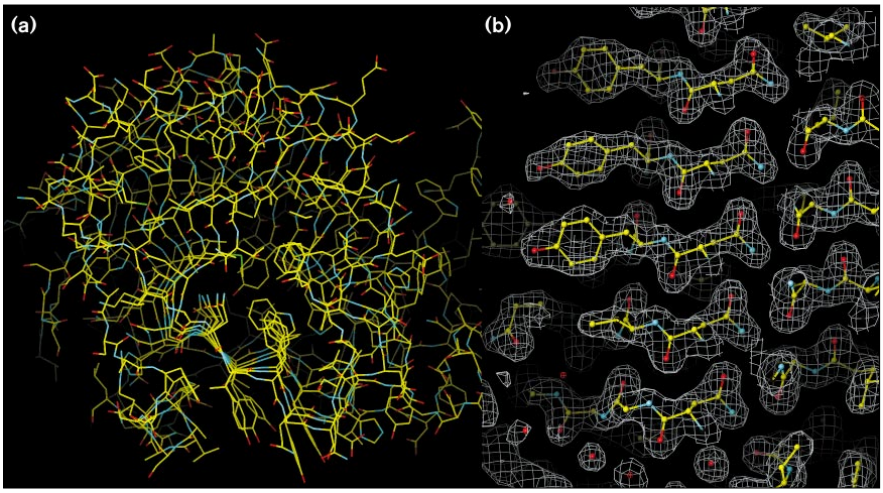

Stacking of residues in the structure of pectin lyase A (4M-147). (a) Perpendicular view of the parallel β helix from the C-terminal end. The core has been aligned along the T2 area, showing the conserved, amphipathic C-terminal helix viewed in cross-section packing against the T2 loop. Attention is drawn to the internal asparagine ladder (part of the T2 loop), the internal aromatic stack and the external cluster of five tyrosine residues. The tyrosine residues form two stacks: one comprising three residues, which pack against the C-terminal helix, and a second, parallel stack consisting of two residues. (b) Detail of the five-membered asparagine ladder and three of the external tyrosine residues. $2F_o–F_c$ electron-density map at 1.93 Å resolution, contoured at 1.4σ. (Figure prepared in O [25].)

Figure 4

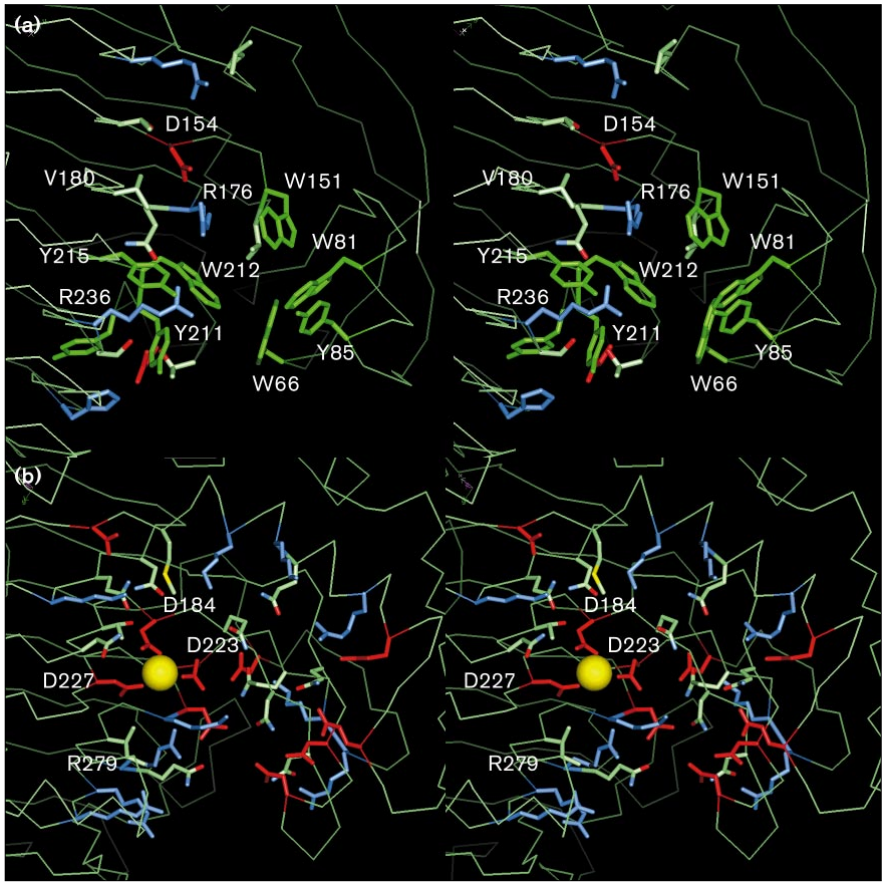

The substrate-binding sites of pectin lyase A and *Bacillus subtilis* pectate lyase. (a) Stereo view of the substrate-binding site of pectin lyase A. Residues Asp154, Arg176 and Arg236 are expected to play a role in catalysis (see text for details). (b) Stereo view of the substrate-binding site of pectate lyase from *B. subtilis* in complex with Ca^{2+}. The sidechains shown have been selected on the basis of their proximity to the substrate-binding cleft. No role in binding or catalysis is implied for these residues, with the exception of Asp184 and Arg279 for which a critical role in catalysis is presumed. Residues coloured red are negatively charged at the pH of catalysis, residues in blue are positively charged and aromatic residues are shown in green; the Ca^{2+} ion is shown as a yellow sphere. (The figure was produced using QUANTA [35].)

molecule. Hence, it could be argued that the N- and C-terminal tails, the asparagine ladder construction, and the *Val*-Trp-*Ile*-Asp-His pattern contribute towards maintaining the parallel β-helix architecture, while diversity around the active site allows variation in substrate specificity. The high structural conservation of the tails corroborates the evolutionary relationship between pectate and pectin lyases.

The substrate-binding site

In the extracellular family of pectate lyases, the cleft formed between the long T3 loops and PB1 has been proposed as the substrate-binding site [7,9,10]. The binding cleft of pectin lyase A differs considerably from those observed in the pectate lyase structures, this contrasts markedly with the notable overall structural similarity.

Pectin lyase A exhibits a cleft dominated by aromatic residues, the charged amino acids being those for which a catalytic role is expected, Asp154, Arg176 and Arg236 (Fig. 4a). The aromatic residues comprise four tryptophans (Trp66, Trp81, Trp151 and Trp212) and three tyrosines (Tyr85, Tyr211 and Tyr215). They do not form stacks but instead three pairs of residues (Trp81–Trp151, Trp66–Trp212 and Tyr211–Trp212) are arranged in edge to face interactions, with the closest approach of the nonhydrogen atoms being 3.5–4.0 Å. These residues are conserved in the other *A. niger* pectin lyases, while the tyrosine residues Tyr85 and Tyr215, do not form similar pairwise interactions and are not conserved. Therefore, it could be inferred that the three aromatic pairs described above contribute to maintain the architecture of the binding cleft. Fluorescence quenching studies using the highly homologous pectin lyase D [13], suggest that one or more of these aromatic residues are involved in substrate binding. It is expected that they contribute to the affinity for methylated pectin as a substrate. Site-directed mutagenesis studies have been performed on hen egg white lysozyme in which the residue Trp62 was replaced with the aliphatic amino acids leucine, isoleucine, valine, alanine and glycine [15]. The results of these studies suggested that aromatic residues favour binding with noncharged polysaccharides when the residue is involved in aromatic ring sugar stacking, one of the frequently observed features of carbohydrate–protein interactions. The presence of a substrate-binding cleft which is rich in aromatic sidechains and favours the binding of the noncharged substrate, highly esterified

Figure 5

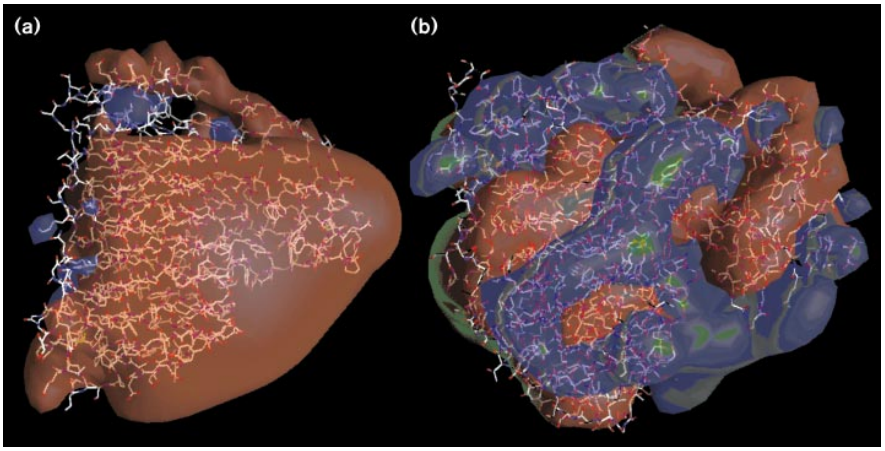

Electrostatic potentials for pectin lyase A and *Bacillus subtilis* pectate lyase (BsPel) calculated using GRASP [36]. The calculation used standard p*K* values and corresponds to pH 7.0. (a) Potentials for pectin lyase A contoured at +12 (blue) and –12 (red) kTe–1. (b) Potentials for BsPel complexed to Ca^{2+} contoured at +2 (blue) and –2 (red) kTe–1, where k is the Boltzmann constant (JK^{-1}), T is the temperature (298K) and e is the charge on an electron (C).

pectin, is consistent with the known specificity of pectin lyase A.

Carbohydrate-binding sites unusually rich in aromatic amino acids have been observed previously. This was reported for an antibody Fab fragment bound to a carbohydrate epitope [16], in which aromatic sidechains dominate the Fab–carbohydrate binding scheme. The relative disposition of tryptophan residues in the pectin lyase A binding site, resembles the arrangement of tryptophans in the Fab–carbohydrate complex.

In sharp contrast, the structures of the pectate lyases determined to date present a substrate-binding region rich in charged acidic and basic residues, suggesting an electrostatic basis for substrate recognition (Fig. 4b). In the Ca^{2+}–BsPel complex, Ca^{2+} binds at the bottom of the substrate-binding cleft to three aspartate residues: Asp184, Asp223 and Asp227 (BsPel numbering). Within the family of extracellular pectate lyases, Asp184 and Asp227 are absolutely conserved, while Asp223 is conservatively substituted by a glutamate. In pectin lyase A, Arg176 corresponds to Asp223, and Val180 is equivalent to Asp227; Asp154 in pectin lyase A corresponds to Asp184 in pectate lyase, being the only conserved carboxylate. The only other residue in the binding cleft to be absolutely conserved across the families of extracellular pectate and pectin lyases is Arg236 (pectin lyase numbering). Assuming that extracellular pectate and pectin lyases evolved from a common ancestral lyase, it might be expected that the two conserved residues, Asp154 and Arg236, play equivalent roles in related mechanisms. However, in pectate lyase the residue equivalent to Asp154 is involved in Ca^{2+} binding.

In a general β-elimination reaction two ionic groups are removed from the substrate: an α proton commonly assisted by a base, and a β-leaving group often assisted by an acid. This reaction results in the formation of a double bond. In enzyme-catalyzed β-elimination reactions, metal ions often appear to play a role in activating the α atom. Pectate lyase requires Ca^{2+} for catalysis but pectin lyase does not. This may reflect the increased stability of the pectate substrate against depolymerization by β elimination. In pectin, the proton at C5 is activated by the electron withdrawing carbonyl group of the carboxymethyl at C6, however, pectate contains carboxylate anions at the C6 position, and is more stable due to the reduced electron withdrawing power of this group. The Ca^{2+} ion in pectate lyase could aid substrate binding by interacting with the carboxylate group at C6, increasing the electron withdrawing effect at C5 and enabling the abstraction of the α proton. This proposed role for Ca^{2+} may explain its absolute requirement for the β-elimination catalysis by pectate lyase, Asp223, a residue that binds Ca^{2+} in pectate lyase, is equivalent to Arg176 in pectin lyase, therefore, it could be suggested that the roles of Ca^{2+} in pectate lyase and the arginine in pectin lyase A are related, both stabilizing negatively charged species. The way in which the active site assists bond cleavage is therefore different in pectate and pectin lyases.

Pectin lyase A is rich in acidic residues, the enzyme from strain N400 contains a total of 48 aspartates and glutamates and the enzyme from strain 4M-147 contains a total of 47 acidic residues. The experimental pI of pectin lyase A from strain N400 is 3.5 [17] and therefore an overall negative charge is expected at the pH of optimum catalysis, 5.5 [13]. A study of the region of the protein surrounding the substrate-binding site, revealed that acidic residues cluster around it in both the parallel β-helix domain and the apex of the main T3 loop. The global effect is a significant negative electrostatic potential, enveloping the substrate-binding site. In contrast, the

Figure 6

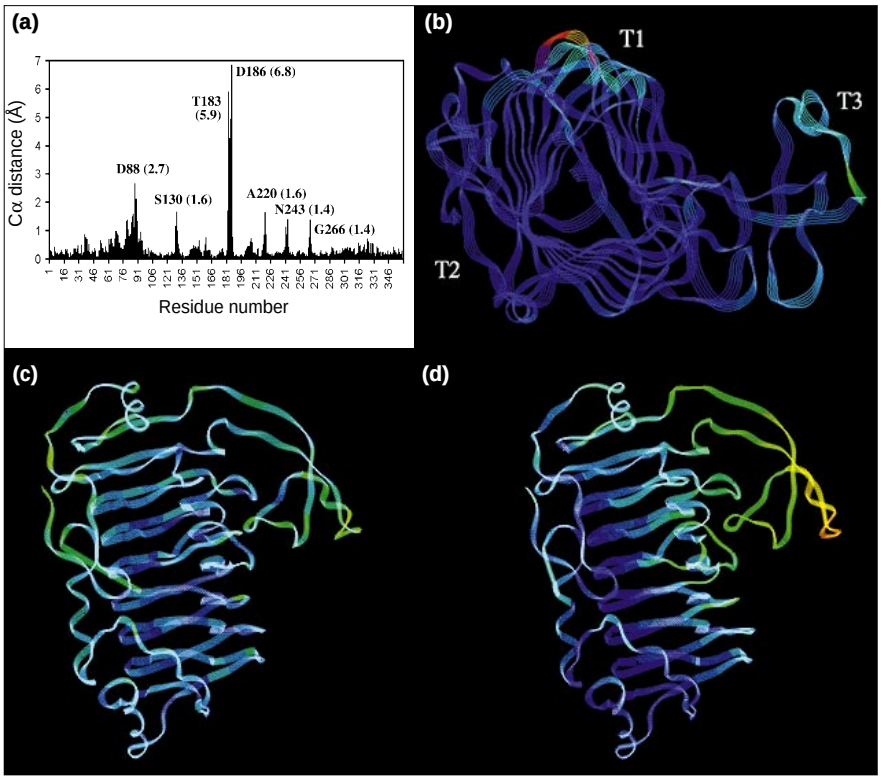

Comparison of the structures of pectin lyase A from strains 4M-147 and N400. (a) Two-dimensional plot showing the distances between equivalent Cα atom positions in the two superimposed pectin lyase structures. Residues presenting maximum local values are labelled and distances, in Å, are specified in parentheses. (b) The equivalent three-dimensional plot. The distances have been plotted on a ribbon following the Cα trace of the protein and coloured in a blue (minimum value) to red (maximum value) gradient. Asp88 appears in green in the T3 loop, and Thr183 and Asp186 are visible in red in the corresponding T1 loop. Variations between the two pectin lyase structures occur in the T1 and T3 regions, while the T2 region and the N- and C-terminal tails are in close agreement. Three-dimensional plots of the temperature factors of the pectin lyase A structures from (c) strain N400, space group P1 and (d) strain 4M-147, space group $P2_12_12_1$; the plots are coloured using a blue-to-red gradient. A common lower cut-off value, set to 15 $Å^2$, has been used for comparison. It can be seen that the structure in space group P1 has a more uniform distribution of temperature factors, while the structure in space group $P2_12_12_1$ has a rigid T2 area and more flexible T1 and T3 loops.

electrostatic field arising in pectate lyase with bound Ca^{2+}, is an elongated ribbon of positive potential (centered at the Ca^{2+} ion) which complements the negatively charged pectate substrate (Figs 5a,b). The different charge distribution of these enzymes may contribute to their substrate specificity, pectate being repelled by the negative charge on pectin lyase but attracted to the positively charged pectate lyase cleft. High ionic strength is needed for pectin lyase to express its full activity and for optimal stability [13]. The substantial negative potential will be attenuated in these conditions, but will still contribute to the binding of methylated rather than demethylated substrate.

Structural differences

Pectin lyase A from strain N400 crystallizes in space group P1 with two molecules per asymmetric unit, while the enzyme from strain 4M-147 gives crystals in space group $P2_12_12_1$. The residues involved in the crystal packing of pectin lyase A from the two strains and the nine amino acid substitutions are illustrated in Figure 2. The differences between the two molecules in the P1 crystal form are sufficiently small that strict noncrystallographic symmetry (NCS) could be successfully used in the refinement; any differences between NCS-related molecules are substantially smaller than the differences between the P1 and the $P2_12_12_1$ structures.

The structures of pectin lyase A from the two strains show major differences that might in principle be caused by sequence changes, different patterns of glycosylation, crystal packing or crystallization conditions (especially pH). Differences in protein conformation can be revealed by calculating the distances between the Cα atoms of equivalent residues in superimposed models (Figs 6a,b). Deviations accumulate in the T1 area and the apex of the long T3 loop, which has higher than average temperature factors in the $P2_12_12_1$ structure (Figs 6c,d). The major structural rearrangement, up to 6.8 Å, affecting residues around Asp186, was identified in the fourth T1 loop.

Compared to pectin lyase A from N400, the enzyme from 4M-147 has a formal excess charge of two (Glu12→Lys, Asp19→Ser and Ala289→Glu) and two fewer cysteine residues, although the same disulphide bridges are formed in both strains. Of the nine substitutions, Cys248→Ala and Phe253→Trp are compensatory changes in the hydrophobic core of the parallel β helix. Residue 253 is one of three aromatic residues forming the aromatic stack of pectin lyase A, the space left by the substitution of tryptophan by the smaller phenylalanine residue is filled by the cysteine which replaces alanine. The other seven substitutions only marginally affect the hydrogen-bonding network and the mainchain conformation remains

Figure 7

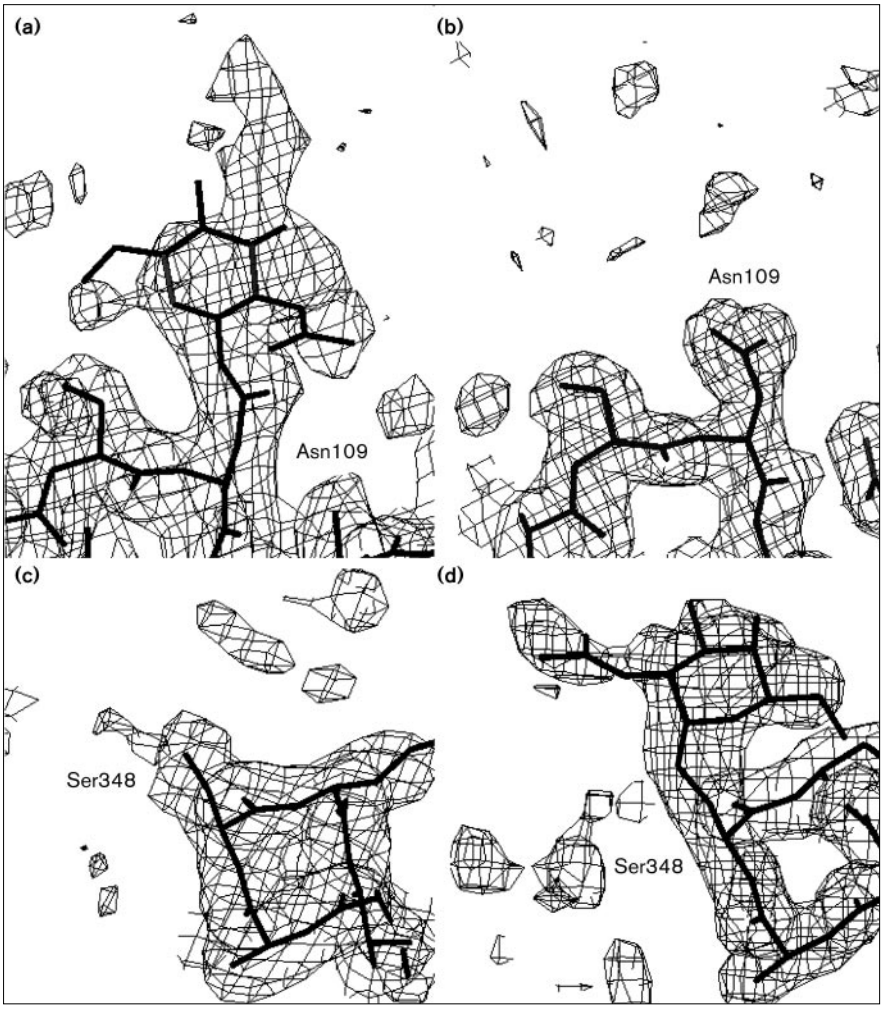

Electron-density maps for the pectin lyase A crystal structures around residues Asn109 and Ser348. The electron density around Asn109 which is glycosylated in strain N400 (P1 structure) (**a**) but not in strain 4M-147 ($P2_12_12_1$ structure) (**b**). The electron density around Ser348 which is not glycosylated in strain N400 (**c**) but is in strain 4M-147 (**d**). The saccharides built into the maps are the commonly occurring *N*- and *O*-linked saccharides. The $2F_o–F_c$ α_{calc} maps are calculated using the protein only (no saccharide or waters included in the model) and are contoured at 0.75σ. The saccharide density is relatively weak but provides clear evidence for different glycosylation patterns in the two structures.

unaltered. Of the substituted residues only the sidechain of residue 317 is involved in a crystal contact (with the carboxylate of Asp324). This intermolecular interaction is conserved between the two crystal forms despite the substitution of serine for cysteine, as both act as a hydrogen-bond donor in this contact. Thus the nine substitutions are probably neither responsible for the different space groups nor for the obvious changes in the conformation of the protein between the two crystal forms, although ionization of Cys317 might prevent the N400 protein crystallizing at high pH.

The observed glycosylation pattern of pectin lyase A in the two crystal forms is different, as observed in the $2F_o–F_c$ electron-density maps. Pectin lyase A strain N400, expressed in *Aspergillus nidulans* and purified [17], has an *N*-glycosylation site at Asn109 and an *O*-glycosylation site at Thr68, whereas pectin lyase A from strain 4M-147 has two *O*-glycosylation sites at Thr68 and Ser348 (Figure 7). As no experimental information on saccharide composition is available, *N*-acetylglucosamine and *N*-acetylgalactosamine have been built into the models according to established *N*- and *O*-glycosylation patterns [18]. However, as the density for the saccharides is poorer than for the protein and does not allow for identification of the specific saccharides, these were included in the models once the refinement was completed and they were not used in the calculation of either electron-density maps or refinement statistics.

The differences in glycosylation might favour the different crystal forms but our electron-density maps do not show the full extent of the oligosaccharide moieties. Asn109 is near a crystal contact in the $P2_12_12_1$ form, implying that extensive glycosylation of the N400 protein might destabilize that form.

Pectin lyase A is optimally active within a limited pH range, between 5.5 and 7.0 depending on substrate concentration and ionic strength [13]. This sharp pH activity profile cannot be easily explained in terms of ionization of

Figure 8

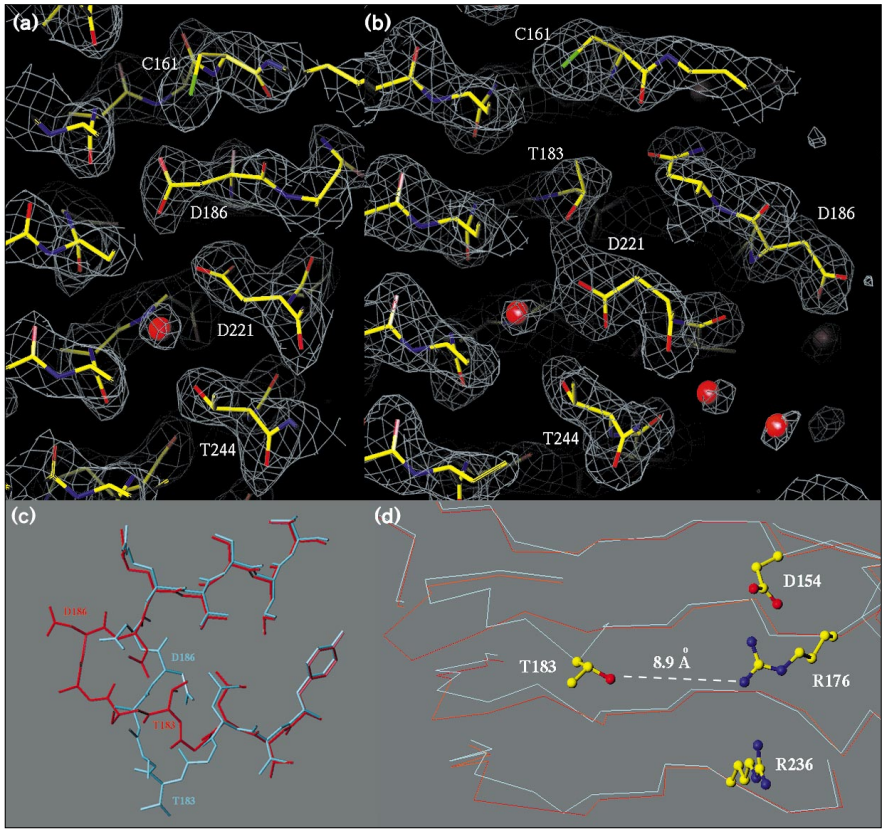

Details of the pH driven conformational change. (a) View of the inner T1 loop area from the structure of pectin lyase A (strain N400) determined at pH 6.5. The illustration follows the longitudinal axis of the parallel β helix. The electron density corresponds to a $2F_o–F_c$ map at 2.4 Å resolution contoured at 1.2σ. Water molecules are shown as red spheres; atoms are in standard colours. (b) View of the equivalent region of the structure from strain 4M-147 at pH 8.5. The $2F_o–F_c$ electron-density map at 1.93 Å resolution contoured at 1.0σ. (c) Cross-sectional view of the fourth T1 loop. The structure at pH 6.5 is shown in cyan and the structure at pH 8.5 is in red. The loop undergoes a conformational change so that Thr183 replaces Asp186 when this residue is no longer facing the inside of the cylinder; residues affected are 182–187. (d) The possible steric effect of pH on substrate binding or catalysis. A longitudinal view of the substrate-binding cleft, colour-coded as in (c). The sidechains of putative catalytic residues are displayed and labelled as is Thr183, which is displaced by the conformational change.

one or more of the putative catalytic residues (Asp154, Arg176 and Arg236, being the only candidates given the aromatic character of the binding cleft). Instead, ionization occurs in an aspartate residue in the T1 loop which forms part of the binding cleft. Pectin lyase A from strain N400 was crystallized at pH 6.5, the pH at which the enzyme is optimally active. The structure at this pH contains two aspartate residues inside the parallel β helix: Asp186 in the fourth T1 loop and Asp221 in the consecutive turn. The distance between the Oδ2 atoms of these two residues is 2.72 Å. This would not be energetically favourable if both residues were deprotonated. Instead, a hydrogen bond must be formed between them, suggesting that one of them is deprotonated but not the other. The pectin lyase A structure solved at pH 8.5 from strain 4M-147, shows Asp221 still inside the core but Asp186 has sprung out and is now exposed to the solvent (Figs 8a,b). It appears, therefore, that residue Asp221 is charged and located permanently inside the β helix; the change observed at high pH can be attributed to the deprotonation of residue Asp186.

At pH 6.5, Asp186 acts to stabilize the charged Asp221 on the inside of the parallel β helix. At pH 8.5, Asp186 is not

Table 2

Hydrogen bonds stabilizing the charged aspartates buried inside the parallel β helix.

Strain N400 (pH 6.5)			Strain 4M-147 (pH 8.5)		
Donor	Acceptor	Distance (Å)	Donor	Acceptor	Distance (Å)
Asp186 N	Asp221 Oδ1	2.89	Thr244 Oγ1	Asp221 Oδ1	2.78
Ala220 N	Asp221 Oδ1	3.12	Asp221 N	Asp221 Oδ1	2.66
Water O	Asp221 Oδ2	2.87	Thr183 Oγ1	Asp221 Oδ2	2.54
Asp186 Oδ2	Asp221 Oδ2	2.72	Water O	Asp221 Oδ2	2.73
Asp160 N	Asp186 Oδ1	3.06			
Cys161 Sγ	Asp186 Oδ1	3.57			

available for this role and the orientation of the sidechains of neighbouring residues, residues 182–187, change to assure the stability of Asp221. Under these conditions, Thr183 interacts with Asp221 to form a short, strong hydrogen bond, the oxygen atoms involved being only 2.54 Å apart. Table 2 lists the hydrogen-bond interactions that stabilize Asp221 inside the core for both T1 conformations. At both pH values residues from the same T1 loop contribute to neutralize the internal Asp221, therefore, structural changes mainly affect one single T1 loop (Fig. 8c). The structures of neighbouring T1 loops are only affected to a minor extent and, although shifts occur, the relative position of groups is maintained. At pH 8.5, a well defined water molecule (B factor = 35.8 $Å^2$) is found in the equivalent position of the carbonyl group of Thr183 in the pH 6.5 structure, preserving the local hydrogen-bonding pattern in the T1 region.

The structural changes observed in the T1 loop region are most likely to be caused by the different pHs of crystallization. This structural rearrangement due to an increase in pH is the most probable cause of the biochemical observation of a reduction in activity. In the active form of the enzyme (pH 6.5), Thr183 is oriented towards the binding cleft and is located approximately 8.9 Å from the catalytic Arg176; at pH 8.5 this space is unoccupied and the surrounding area is somewhat altered (Fig. 8d). Therefore, it is more likely that the effect on catalysis is a steric effect, in which binding of the substrate is affected either directly or by perturbing the water structure of the active site.

The long T3 loop shows a small rigid-body movement between the two crystal forms. Both forms show crystal contacts with this loop but the P1 crystal makes more contacts near the apex of the loop, and is significantly better defined than in the $P2_12_12_1$ space group, as characterized by higher than average temperature factors (Fig. 6c).

Biological implications

Pectin and pectate lyases are virulence factors that degrade the pectic component of the plant cell wall. The majority of pectate and pectin lyases, including those of known structure, comprise a family of enzymes that have evolved from a common ancestor although some of the members have diverged notably. *Aspergillus niger* pectin lyase A and *Bacillus subtilis* pectate lyase show 17% sequence identity after structural alignment, and represent two distinct specificities. The structure of pectin lyase A, described here, has established the structural basis for the substrate specificity of these two lyases and provides an understanding of the pH and ionic strength dependence of pectin lyase activity.

The structures of pectin and pectate lyases determined to date, show the parallel β-helix fold. Structural conservation is greatest in a region which is remote from the active site, while the extent of divergence in the substrate-binding cleft is remarkable, reflecting the substantial differences in the nature of their respective substrates. Pectate is highly charged, binds Ca^{2+}, does not readily loose its C5 proton and is only cleaved by pectate lyase. Conversely, fully methylated pectin is less polar, more susceptible to degradation, does not readily bind metal ions and is only cleaved by pectin lyase. The binding sites of the two lyases, therefore, reflect the different requirements for substrate binding and catalysis. Pectate lyase presents a binding cleft rich in charged amino acids with no aromatic residues and uses Ca^{2+} in catalysis, as an aid for the activation of the C5 proton. In contrast, pectin lyase has a cleft dominated by aromatic residues, with the residues Asp154, Arg176 and Arg236 being the only potential catalytic groups. Pectin lyase does not require Ca^{2+} for catalysis but Arg176 may play a similar role. Substrate specificity is not only a consequence of the hydrophobicity of the binding cleft, but also of long-range electrostatic effects. The negative electrostatic potential surrounding the pectin lyase substrate-binding cleft tends to repel the negatively charged pectate which is not a substrate. Conversely, the positive potential surrounding the pectate lyase substrate-binding cleft attracts the demethylated, pectate substrate. The electrostatic effect will be modulated by the salt in the medium, high ionic strength being necessary for the activity of pectin lyase. It can be concluded that, while still sharing a common architecture and a related mechanism, these enzymes diverge significantly in their carbohydrate binding strategy.

The reduction in pectin lyase activity above neutral pH is not explained by the p*K*as of the sidechains at the active site, rather it is due to a pH triggered conformation change. The more active, low pH form of the enzyme contains two buried aspartic acid sidechains within the parallel β helix. These two residues are in close contact, suggesting that one aspartate, Asp221, is ionized and accepts a hydrogen bond from the second uncharged aspartate, Asp186. On raising the pH, Asp186 becomes ionized, can no longer be accommodated adjacent to Asp221 and becomes exposed to the solvent. Under these conditions, Asp186 is replaced by a threonine residue, Thr183, which was previously solvent-exposed in the active-site cleft at low pH, thus changing the shape of the substrate-binding cleft.

Pectins have traditionally been used in the food industry for their functional properties: gelation, viscosity and stabilization. They are extracted from apple pomace and citrus peel and processed using inorganic acids and bases. Protein engineering of these enzymes offers the advantages of faster processing and more specific cleavage patterns giving greater control of the structure of the processed pectins and improved functionality.

Materials and methods

Cloning and sequencing

The amino acid sequence of pectin lyase A from *A. niger* strain N400 was obtained from GenBank (accession code X60724 [17]). To determine the complete sequence of strain 4M-147 pectin lyase A the structural gene was cloned. Primers, for use in the polymerase chain reaction (PCR), were based on the reverse translation of the experimentally determined protein sequences; the primers were synthesized and used to amplify genomic DNA. The corresponding PCR fragment was cloned and subsequently used as a probe to identify a genomic clone carrying the entire structural gene.

Genomic DNA from *A. niger* strain 4M-147 (culture collection of Danisco Ingredients, Brabrand, Denmark) was extracted from mycelium. SURE, XL1-Blue and XLOLR *Escherichia coli* strains, the vector lambda ZAP Express and pBluescript, and the filamentous helper phage ExAssist were all purchased from Stratagene, UK. The nucleotide sequence of the forward primer (PL1) was derived from the internal peptide sequence Ala-Glu-Gly-Phe-Ala-Lys-Gly-Val-Thr which features one of the amino acid substitutions characteristic of pectin lyase A from strain 4M-147. The reverse primer (PL2) corresponded to the internal sequence Gly-Ala-Ile-Lys-Gly-Lys-Gly. A PCR product of approximately 400 base pairs (bp) was gel-purified from a mixture of bands and cloned, blunt-ended, into the *Eco*RV site of pBluescript. The nature of this clone was checked by DNA sequencing. Chromosomal DNA was partially digested with *Sau3*AI and the resulting DNA fragments were size fractionated. Fragments in the range 2.5–8 kb were purified and ligated into *Bam*HI-digested lambda ZAP Express. The library was constructed using XL1-Blue cells as indicated by the manufacturer. This library was screened with a ^{32}P-labelled DNA insert liberated from the pBluescript clone with *Bam*HI and *Hin*dIII. After three rounds of plaque screening four positive lambda clones were isolated and the recombinant plasmids recovered following excision with the filamentous phage ExAssist, as indicated by the manufacturer.

A single clone carrying the entire gene on a 3 kb insert was selected for DNA sequencing. The complete sequence of the clone in both strands was determined by cycle sequencing using universal and custom primers employing dye-terminator chemistry with an ABI 373 automated DNA sequencer. The nucleotide sequence of the clone revealed a gene of 1349 bp including four introns, which are conserved in location when compared to the sequence reported for strain N400. The encoded protein has 379 amino acids including 20 amino acids signal sequence to yield a mature protein of molecular weight 38 012 daltons.

Crystallization and X-ray data collection

Pectin lyase A from *A. niger* 4M-147 was crystallized from 28% PEG 4000, 0.1 M sodium acetate and buffered with 0.1 M Tris-HCl at pH 8.5 [19]. The crystals belong to the space group $P2_12_12_1$ with unit cell dimensions of a = 45.4 Å, b = 83.5 Å, c = 93.4 Å; the crystals contain one molecule of protein per asymmetric unit and the solvent content is 47%. Data were collected to 1.93 Å using the large MAR image plate on the wiggler beamline PX 9.6 at the SRS (Daresbury Laboratory). Phase information was obtained from three data sets corresponding to methyl mercury chloride (MMC), ethyl mercurithiosalicylate (EMTS) and uranyl acetate (UO_2Ac_2) derivatives.

Aspergillus niger N400 pectin lyase A was expressed in *Aspergillus nidulans* [17] and crystallized using the hanging-drop method, over 1 ml reservoirs in Linbro trays. Crystallization conditions were surveyed by the protocol of Jancarik and Kim [20], using both crystal screens I and II supplied by Hampton Research. Crystals suitable for data collection were obtained from hanging drops containing 4 μl of protein at 19 mg ml^{-1} in water and 2 μl of reservoir which consisted of 28% PEG 6000, 0.1 M sodium cacodylate buffer at pH 6.5 and 0.2 M sodium acetate. Crystals belong to the space group P1, with unit cell dimensions a = 47.9 Å, b = 52.4 Å, c = 76.3 Å, α = 78.6°, β = 90.1°, γ = 104.6°; there are two molecules per asymmetric unit and a solvent content of 48%. The NCS between the two molecules is given by the Eulerian angles $\theta_1 = 0.0°$, $\theta_2 = 180.0°$ and $\theta_3 = 0°$ (Eulerian axes and angles follow X-PLOR conventions). The two molecules in the asymmetric unit are related by a pseudo-2_1 axis parallel to a. The rotational component is a twofold rotation and the translational component is approximately 0.6 a (fractional).

Table 3

X-ray diffraction data for native pectin lyase A.

Source	*A. niger* 4M-147	*A. niger* N400
Space group	$P2_12_12_1$	P1
Unit cell		
a, b, c (Å)	45.4, 83.5, 93.4	47.9, 52.4, 76.3
α, β, γ (°)		78.6, 90.1, 104.6
Molecules/asymmetric unit	1	2
Maximal resolution (Å)	1.93	2.4
Number of observations	80 561	44 141
Number of unique reflections	25 730	23 252
$R_{sym}(I)$ (%)*	6.5	5.8
Completeness (%)	96.4	81
Completeness (outer shell)(%)	84.3†	92.2‡
$R_{sym}(I)$ (outer shell) (%)*	27.0†	12.5‡
Multiplicity (outer shell)	2.5†	1.5‡

*$R_{sym}(I) = \Sigma_{hkl}\Sigma_i|I_i(hkl) - <I(hkl)>|/\Sigma_{hkl}\Sigma_i I_i(hkl)$. †Data for the outer shell (1.93–2.0 Å). ‡Data for the outer shell (2.8–2.9 Å); additional data were collected to 2.4 Å and were included in the refinement (see text for details). For data in the range 2.4–2.8 Å, the completeness was 59.7% with an $R_{sym}(I)$ of 14.4% and multiplicity of 1.1.

Data were collected from native N400 crystals using a Xentronics area detector and a three-axis camera with CuK_α radiation from a rotating-anode generator equipped with a graphite monochromator running at 40 kV and 80 mA. A single native crystal was used with the data collected in three sweeps with φ at 0°, 60° and 120°. A swing angle (2φ) of 15° and distance of 120 mm was used for the first sweep allowing data to a maximum resolution of 2.4 Å to be recorded. The subsequent two runs were collected at a swing angle of 10° and a distance of 100 mm corresponding to a maximum resolution of 2.8 Å. Accordingly, the completeness and multiplicity are high at 2.8 Å and fall towards the 2.4 Å limit. A derivative data set was collected after soaking the same crystal in 10 mM EMTS in the capillary for 45 min. After removal of the excess liquid, data were collected in two sweeps of 180° in ω with φ at 0° and 90°. The swing angle was 5° with a distance of 120 mm corresponding to a maximum resolution of 3.1 Å.

For both the 4M-147 and N400 pectin lyase A crystals, details on the native data sets and experimental phases are provided in Tables 3 and 4, respectively.

Structure determination and refinement

The structure of pectin lyase A was solved by a combination of MR, MIR and intercrystal averaging techniques.

First, a MR solution for the single molecule in the asymmetric unit of the $P2_12_12_1$ cell was sought using the program AMoRe [21,22]. Search models were derived from the distantly related pectate lyase, BsPel, which shares 17% structure-based sequence identity with pectin lyase. The best solution was obtained from a model lacking the long T3 loops (295 residues remained), using 10–4 Å resolution range and a 22 Å Patterson radius. The solution had a correlation coefficient of 0.322 and an R factor of 51.9% after rigid-body refinement within AMoRe. Initial MR phases were too inaccurate to provide a workable starting point for refinement, however, they were used successfully to phase difference Fouriers enabling the positions of the

Table 4

Heavy-atom phasing.

	2 mM EMTS* (140 min)	0.5 mM MMC* (60 min)	4 mM UO_2Ac_2* (130 min)	10 mM EMTS† (45 min)
Detector	Fuji image plate Weissenberg camera (Photon Factory)	Fuji image plate Weissenberg camera (Photon Factory)	Large MAR (LURE)	Area detector (Siemens)
Maximum resolution (Å)	2.24	3.0	2.0	3.1
Number of observations	58 310	13 976	69 831	24 971
Number of reflections‡	17 954	4408	22 913	11 117
Completeness (%)	93.4	59.7	92.4	76
$R_{sym}(I)$ (%)§	6.1	7.1	5.8	5.5
R_{iso} (%)#	11.1	17.4	35.9	10.3
Phasing power¶	0.78 (<4 Å)	1.38 (<4 Å)	1.00 (<4 Å)	1.28 (<3.1 Å)
R_{cullis} (%)¥	91 (<4 Å)	79 (<4 Å)	87 (<4 Å)	87 (<3.1 Å)
Sites per molecule	1	1	4	1

EMTS is ethyl mercurithiosalicylate and MMC is mercury methyl chloride. *Heavy-atom derivatives for the $P2_12_12_1$ space group. †Heavy-atom derivative obtained for the P1 crystal form. ‡Number of unique h,k,l. §$R_{sym}(I) = \Sigma_{hkl} \Sigma_i |I_i(hkl) - <I(hkl)>| / \Sigma_{hkl} \Sigma_i I_i(hkl)$. #$R_{iso} = \Sigma ||F_P| - |F_{PH}|| / \Sigma |F_P|$, where F_P is the native and F_{PH} is the derivative structure-factor amplitude. ¶Phasing power is $<F_H>/<_E>$, where $<F_H>$ is the root mean square (rms) calculated heavy-atom structure factor and <E> is the rms lack of closure error. ¥$R_{cullis} = \Sigma ||F_{PH} - F_P| - F_H| / \Sigma |F_{PH} - F_P|$, where F_H is the calculated heavy-atom structure-factor amplitude, F_P and F_{PH} are the native and derivative structure-factor amplitudes, respectively. Phases were calculated to 4.0 Å except for the EMTS soak using P1 crystals where phases were calculated to 3.1 Å, as indicated in the table.

heavy atoms to be determined. Experimental phase information was obtained from three heavy-atom derivatives: MMC (one single binding site also identified by isomorphous difference Patterson), and EMTS (same binding site as the MMC derivative) and UO_2Ac_2 (four sites).

Phases from the derivatives were refined with MLPHARE [22,23] and combined with model phases using SIGMAA [22,24]. Several cycles of manual rebuilding in O [25] and positional refinement in X-PLOR [26] yielded a partial model for most of the parallel β-helix domain (R factor = 47.2%, R_{free} = 50.8%). The PB sheets could be defined and their sequence assigned, but there was no density for most of the loops. Poly-alanine fragments, representing the N and C termini, were misplaced in comparison to the final model, and the 40-residue long T3 loop, was totally absent from the electron density.

Only using this partial model could a MR solution be obtained for the P1 crystal form. The model, tested at a resolution range of 15–4 Å and a Patterson radius of 22 Å in AMoRe, yielded a best solution for the two molecules in the P1 cell with a correlation coefficient of 0.409 and R factor of 50.5% after rigid-body refinement within AMoRe. In addition, experimental phases were obtained from an EMTS derivative. The isomorphous difference Patterson gave the vector between the two heavy-atom sites in the cell (one per molecule), and a difference Fourier using the MR phases located a consistent pair of heavy-atom sites. For each space group, maps were calculated using combined MR and MIR phases. From there on intercrystal averaging (three copies) was exploited through the use of real-space averaging using the MAVE software [27], with mask creation and manipulation using the MAMA software [28]. Recursive cycles of manual rebuilding in averaged maps to 3.0 Å resolution allowed completion of the partial pectin lyase model. In each step, refinement was against the $P2_12_12_1$ data set, while the P1 data were used for cross-validation. In the final stages of refinement, when no improvement could be obtained through averaging, the $P2_12_12_1$ and P1 models were refined independently.

Refinement consisted of molecular dynamics by the method of slow-cool simulated annealing as implemented in X-PLOR [29]. Engh and Huber parameters and topology [30] were used. The reflection data were divided into a working set (95% of the data) and a test set (5% of the data) using the FREERFLAG program [31,22]. Refinement against data from the P1 crystal form utilized bulk solvent correction, overall anisotropic B-factor scaling, strict NCS and grouped B-factor refinement within X-PLOR. Refinement of the $P2_12_12_1$ model involved bulk solvent correction, overall anisotropic B-factor scaling and restrained isotropic B factors for every atom. For the $P2_12_12_1$ data, reflections under 15 Å resolution were discarded due to image plate saturation. Solvent molecules were found using the program ARP [32] in restrained mode and added to the protein model for a final cycle of refinement. Water molecules were checked visually in $2F_o–F_c$ and $F_c–F_o$ electron-density maps using O. Those water molecules with unacceptable hydrogen-bond patterns or temperature factors over 60 $Å^2$ were discarded. During refinement, models were routinely assessed using PROCHECK [33]. The final structures include all 359 residues of the mature protein and have good stereochemistry and geometry as assessed by PROCHECK [33]. Refinement statistics and geometrical parameters for the final models are presented in Table 1.

Accession numbers

The coordinates and structure factors have been deposited in the Brookhaven Protein Data Bank with accession codes 1IDJ and 1IDK for *A. niger* strain N400 and 4M-147, respectively.

Acknowledgements

We would like to thank our colleague Leila Lo Leggio for assistance in data collection. We are also grateful to Colin Nave (SRS), Roger Forme (LURE) and Professor Sakabe (Photon Factory) for allocation of beamtime and support during collection. This work is supported by the BBSRC, MAFF and European Community.

References

1. Pilnik, W. & Rombouts, F.M. (1981). Pectic enzymes. In *Enzymes and Food Processing*. (Birch, G.G., Blakebrough, N. & Parker, K.J., eds), pp. 105–128, Applied Science Publishers Ltd., London, UK.
2. Wing, R.A., Yamaguchi, J., Larabell, S.K., Ursin, V.M. & McCormick, S. (1989). Molecular and genetic characterization of two pollen-expressed genes that have sequence similarity to pectate lyases of the plant pathogen *Erwinia*. *Plant Mol. Biol.* **14**, 17–28.

3. Rafnar, T., Griffith, I.J., Kuo, M.C., Bond, J.F., Rogers, B.L. & Klapper, D.G. (1991). Cloning of *Amb aI* (antigen E), the major family of short ragweed pollen. *J. Biol. Chem.* **266**, 1229–1236.
4. Collmer, A. & Keen, N.T. (1986). The role of pectic enzymes in plant pathogenesis. *Annu. Rev. Phytopathol.* **24**, 383–409.
5. Barras, F., van-Gijsegen, F. & Chatterjee, A.K. (1994). Extracellular enzymes and pathogenesis of soft-rot *Erwinia*. *Annu. Rev. Phytopathol.* **32**, 201–234.
6. Whitaker, J.R. (1990). New and future uses of enzymes in food processing. *Food Biotechnol.* **4**, 669–697.
7. Henrissat, B., Heffron, S.E., Yoder, M.D., Lietzke, S.E. & Jurnak, F. (1995). Functional implications of structure-based sequence alignment of proteins in the extracellular pectate lyase superfamily. *Plant Physiol.* **107**, 963–976.
8. Yoder, M.D., Keen, N.T. & Jurnak, F. (1993). New domain motif: the structure of pectate lyase C, a secreted plant virulence factor. *Science* **260**, 1503–1507.
9. Lietzke, S.E., Yoder, M.D., Keen, N.T. & Jurnak, F. (1994). The three-dimensional structure of pectate lyase E, a plant virulence factor from *E. chrysanthemi*. *Plant Physiol.* **106**, 849–862.
10. Pickersgill, R., Jenkins, J., Harris, G., Nasser, W. & Robert-Baudouy, J. (1994). The structure of *Bacillus subtilis* pectate lyase in complex with calcium. *Nat. Struct. Biol.* **1**, 717–723.
11. Crawford, M. & Kolattukudy, P.E. (1987). Pectate lyase from *Fusarium solani* f. sp. pisi: purification, characterization, *in vitro* translation of the mRNA, and involvement in pathogenicity. *Arch. Biochem. Biophys.* **258**, 196–205.
12. Kita, N., Boyd, C.M., Garrett, M.R., Jurnak, F. & Keen, N.T. (1996). Differential effect of site-directed mutations in PelC on pectate lyase activity, plant-tissue maceration, and elicitor activity. *J. Biol. Chem.* **43**, 26529–26535.
13. Van Houdenhoven, F.E.A. (1975). Studies on pectin lyase. PhD thesis. Agricultural University, Wageningen, The Netherlands.
14. Jurnak, F., Yoder, M.D., Pickersgill, R. & Jenkins, J. (1994). Parallel β domains: a new fold in protein structures. *Curr. Opin. Struct. Biol.* **4**, 802–806.
15. Maenaka, K., Kawai, G., Watanabe, K., Sunada, F. & Kumagai, I. (1994). Functional and structural role of a tryptophan generally observed in protein–carbohydrate interaction. *J. Biol. Chem.* **269**, 7070–7075.
16. Cygler, M., Rose, D.R. & Bundle, D.R. (1991). Recognition of a cell-surface oligosaccharide of pathogenic *Salmonella* by an antibody Fab fragment. *Science* **253**, 442–445.
17. Kusters-van Someren, M.A., Harmsen, J.A.M., Kester, H.C.M. & Visser, J. (1991). Structure of the *Aspergillus niger pelA* gene and its expression in *Aspergillus niger* and *Aspergillus nidulans*. *Curr. Genet.* **20**, 293–299.
18. Allen, H.J. & Kisalius, E.C. (1992). *Glycoconjugates. Composition, Structure and Function.* Marcel Dekker, Inc., NY, USA.
19. Jenkins, J., *et al.*, & Gravesen, T. (1996). Crystallization and preliminary X-ray analysis of pectin lyase A from *Aspergillus niger*. *Acta Cryst. D* **52**, 402–404.
20. Jancarik, J. & Kim, S.H. (1991). Sparse matrix sampling: a screening method for crystallization of proteins. *J. Appl. Cryst.* **24**, 409–411.
21. Navaza, J. (1994). AMoRe — an automated package for molecular replacement. *Acta Cryst. A* **50**, 157–163.
22. Collaborative Computational Project No. 4. (1994). The CCP4 suite: programs for protein crystallography. *Acta Cryst. D* **50**, 760–767.
23. Otwinowski, Z. (1991). Maximum likelihood refinement of heavy-atom parameters. In *Isomorphous Replacement and Anomalous Scattering*. (Wolf, W. & Leslie, A.G.W., eds), pp. 80–86, SERC Daresbury Laboratory, Warrington, UK.
24. Read, R.J. (1990). Structure-factor probabilities for related structures. *Acta Cryst. A* **46**, 900–912.
25. Jones, T.A., Zou, J.-T., Cowan, S.W. & Kjeldgaard, M. (1991). Improved methods for building protein models in electron-density maps and the location of errors in these maps. *Acta Cryst. A* **47**, 110–119.
26. Brünger, A.T. (1992). *X-PLOR, Version 3.1. A System for X-ray Crystallography and NMR*. Yale University, New Haven, CT, USA.
27. Kleywegt, G.J. & Jones, T.A. (1994). Halloween — masks and bones. In *From First Map to Final Model*. Daresbury Study Weekend Proceedings.
28. Kleywegt, G.J. & Jones, T.A. (1993). Masks made easy. *ESF/CCP4 Newsletter* **28**, 56–59.
29. Brünger, A.T., Kuriyan, J. & Karplus, M. (1987). Crystallographic R factor refinement by molecular dynamics. *Science* **235**, 458–460.
30. Engh, R.A. & Huber, R. (1991). Accurate bond and angle parameters for X-ray protein-structure refinement. *Acta Cryst. A* **47**, 392–400.
31. Brünger, A.T. (1992). Free R value: a novel statistical quantity for assessing the accuracy of crystal structures. *Nature* **355**, 472–475.
32. Lamzin, V.S. & Wilson, K.S. (1993). Automated refinement of protein models. *Acta Cryst. D* **49**, 129–147.
33. Morris, A.L., MacArthur, M.W. & Thornton, J.M. (1992). Stereochemical quality of protein structure coordinates. *Proteins* **12**, 345–364.
34. Kraulis, P.J. (1991). MOLSCRIPT: a program to produce both detailed and schematic plots of proteins. *J. Appl. Cryst.* **24**, 946–950.
35. QUANTA 4.0. (1994). Molecular Simulations Inc. 16, New England Executive Park, Burlington, MA, 01803-5297. USA.
36. Nicholls, A., Bharadwaj, R. & Honig, B. (1993). GRASP: graphical representation and analysis of surface-properties. *Biophys. J.* **64**, 166.